RSC Advances

ROYAL SOCIETY OF CHEMISTRY

www.rsc.org/advances

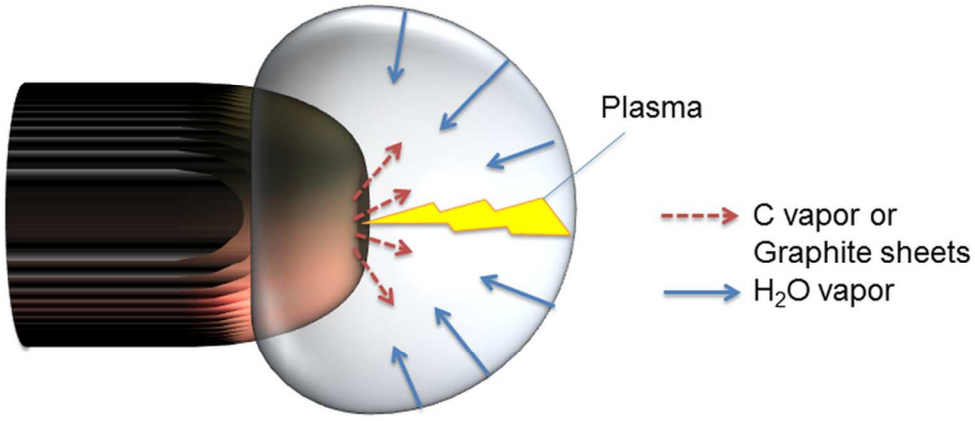

Proposed mechanisms for the bubble formation on the graphite electrodes discharged in distilled water.
91x40mm (300 x 300 DPI)

Solution Plasma Exfoliation of Graphene Flakes from Graphite Electrodes

Hoonseung Lee [1], Maria Antoaneta Bratescu[2], Tomonaga Ueno [1,4], Nagahiro Saito [1,2,3,4,*]

[1] Graduate School of Engineering, Nagoya University, Nagoya 464-8603, Japan

[2] Aichi Science and Technology Foundation, 1267-1 Akiai, Yakusa, Toyota, 470-0356, Japan

[3]Institute of Innovation for Future Society, Nagoya University, Nagoya 464-8603, Japan

[4] CREST, Japan Science and Technology Agency, Tokyo, 102-0076, Japan

Email : hiro@rd.numse.nagoya-u.ac.jp, Tel & Fax : +81 52 789 3259

ABSTRACT

Graphene flakes were successfully produced by a simple method named solution plasma process. The plasma was generated between two carbon electrode tips which were immersed in distilled water. The production approach is a continuous energy accumulation induced by focusing of plasma streamers on the surface of electrodes. This focused energy makes thermal gradient zones where a proper energy level is produced. Concisely, the energy is enough to extract graphene layers from the graphite structure but not enough to break covalent C–C bonds within the graphene sheets. Optical emission spectroscopy results showed the decomposition of carbon from the graphite electrodes with different intensities of the carbon species. Transmission electron microscopy images confirmed hexagonal honeycomb structure of the graphene flakes. Furthermore, broadening of the 2D band in the Raman spectra revealed that the graphene flakes were disordered multilayers.

Keywords graphene flake – low temperature plasma – carbon exfoliation

1. Introduction

Graphene, an allotrope of carbon whose structure is a single planar sheet of carbon atoms arrayed in a honeycomb pattern, has attracted considerable interest from many researchers over the past decade. Since Novoselov et al.[1] have introduced graphene exfoliation technique from graphite using a simple duct tape ('scotch tape' or 'peel-off' method) in 2004, its superior properties such as extremely high mechanical strength[2], large specific surface area[3] high transparency[4,5] and high thermal conductivity[6] have been intensively studied. Based on these properties, graphene is an alternative material for touch screens, capacitors, fuel cells, batteries, sensors, transparent conductive films, high-frequency circuits, toxic-removal materials, and flexible electronics.[4,7-9]

In addition to the peel-off method, graphene was fabricated by chemical methods such as chemical vapor deposition (CVD) and chemical exfoliation. The growth by CVD method provides graphene with excellent electronic conductivity although the method has the disadvantage of potential contamination on the surface by different organic compounds, which were commonly applied during the transfer on the target substrate.[10-13] Graphene fabricated by chemical exfoliation satisfies the cost and mass production requirements for industrial use,[14-16] especially in the application of printed electronic devices due to its stability in solution.[17,18] However, the material can barely be used in large area electronic panels and the conductivity is low compared to that of the CVD-graphene because many defects are produced during exfoliation process.[19]

Nanocarbon allotropes as nanofibers and multiple- or single tubes are usually synthesized in low temperature plasma, plasma assisted CVD, and arc discharges. Plasma-assisted growth and processing of graphene in recent years offer the possibility to synthesize graphene at lower temperatures. The use of plasma for graphene synthesis is quite challenging since it is necessary to simultaneously deliver small amounts of precursors and enable fast and uniform nucleation, while avoiding any damage due to ion bombardment.[20,21] Magnetically enhanced arc discharge has been used for the production and separation of graphene flakes and single wall nanotubes during one-step process.[22]

Another important physical approach to synthesize nanocarbon allotropes is the application of electrical discharge in liquid where the carbon precursor can be either the electrode material or the

liquid media. Carbon onions,[23] carbon nanohorns and nanotubes,[24-27] and metal nanoparticles covered by carbon[28-29] were synthesized in plasma surrounded by a liquid.

Generally, Van der Waals forces between graphite layers are weak and significantly smaller than that of covalent C–C chemical bonds in the planes. Thus in order to produce graphene from graphite, it is important to control the energy during the process so that the Van der Waals force between the layers is overcome but the molecular structure consisting of the covalent C–C bonds remains intact. The energy of the conventional arc plasma exceeds the C–C bond energy and results in the destruction of both interlayer bonding and molecular structure of the graphite. Low-energy plasma in liquid phase may selectively overcome the Van der Waals force while maintaining the aromatic structure. Therefore well-controlled plasma in liquid may exfoliate graphene from graphite electrode without creating many defects in the structure. In this paper low-energy plasma in liquid termed solution plasma process (SPP) was used for the graphite exfoliation.

SPP is a non-equilibrium, cold plasma that induces extremely rapid reactions by the present of reactive chemical species, radicals, and UV radiation. SPP can be carried out at atmospheric pressure, within the glow discharge limits, and it permits a good level of control to be exerted over the chemical reactions.[30,31] The process has been reported as an innovative and simple method for the synthesis of various nanoscale materials.[32-36] In this study, low-energy plasma in the liquid phase is the most important characteristic that allow the synthesis of graphene flakes in water by the SPP exfoliation.

2. Experimental procedure

A schematic representation of the experimental setup is shown in Fig. 1. Graphite electrodes with purity of 99.9999% (Nilaco Co. Ltd.) were used as carbon precursor. The tips of the electrodes were cut in round-edge cone shape from 3 mm of the edge. The diameter of the electrodes was 3 mm and the inter-electrode gap was 0.5 mm. The discharge was generated in a beaker between two graphite electrodes using a bipolar pulsed power supply (MPS-R06K010-WP1-6CH; Kurita Co. Ltd.) operating at a voltage from 1 to 2 kV, a frequency from 10 to 60 kHz, and a pulse width from 1 to 4 μs, in distilled water with 0.06 μScm^{-1} conductivity. Due to aggregation, the samples (carbon materials) were resuspended in ethanol before carrying out the analysis.

The obtained nanocarbon materials were measured by Raman spectroscopy. The samples were prepared by blending with ethanol prior to drop on a silicon wafer. After the sample was dried, visible Raman spectroscopy was conducted at room temperature using a 532.5 nm laser (NRS-1000; JASCO). The laser power used for nanocarbon material analysis was 10 mW. Rayleigh scattering was eliminated by a notch filter with 100 cm^{-1} bandwidth. The Raman spectra were collected in different points within an area of about 1 mm^2.

The morphology and selected area electron diffraction (SAED) of the nanocarbon materials were observed by transmission electron microscopy (TEM) (JEM-2500SE; JEOL) with 200 kV accelerating voltage. Samples for the TEM analysis were prepared by placing a drop of ethanol containing the carbon material on a holey Cu TEM grid. During TEM observation, the information of the suspended carbon materials on the edge of the amorphous carbon film from the Cu grid was carefully collected. The high resolution TEM (HRTEM) was performed by recording the images close to the Scherzer defocus and the sample height was adjusted to keep the objects focused in the optimum lens current. A beam current density of ~10 A cm^{-2} used for HRTEM observation using a CCD camera brings a temperature increase for a few degrees. This amount of beam current was reported to have little influence to the samples.[34] The differences between carbon structure were obtained from the electron energy loss spectroscopy (EELS) measurements of the carbon edge at 284 eV in HRTEM mode using a Gatan Imaging Filtering device operated by Filter Control and Digital Micrograph software. The EELS spectra were recorded with 0.2 eV per pixel and 2 mm aperture.

Time-averaged optical emission spectra (OES) of the discharge were observed with an optical spectrometer (HR2000+CG-UV-NIR; Ocean Optics) through a 5 mm diameter quartz window in the spectral range from 200 to 1100 nm and a resolution of 0.1 nm.[37] The discharge voltage and current were monitored using a high-voltage probe (P6015A; Tektronix) and a current probe (model 6595; Pearson Electronics), respectively, on an oscilloscope (DS1202CA; RIGOL). During the synthesis, the liquid temperature was measured with an alcohol thermometer.

3. Results and discussion

3.1 *Nanocarbon structure and morphology analysis*

Fig. 2 shows a schematic graph of the structural changes of the nanocarbon materials in dependence with the frequency and pulse width of the applied high voltage. Low energy discharges, which were generated at low frequency and low pulse width led to the formation of graphene flakes, whereas high energy discharges generated carbon onion structures. In the middle range, both graphene flakes and carbon onions were observed. Study on various methods of graphite exfoliation in liquid phase, for example, for graphene-ink preparation[38], and dispersion of graphene in water-surfactant solutions[39] have shown that the defects in graphene sheets were related to the edges but not to the structural changes as occurs in the SPP.

Typical TEM, HRTEM and SAED images are shown in Fig. 3(a)–(f). Spherical carbon onions are shown in Fig. 3(a)–(c) and plain layered graphene flakes are shown in Fig. 3(d)–(f). The multiple nested onion-like particles displayed in Fig. 3(a) have diameters from 2 to 16 nm. In the case of graphene flakes, a large quantity was observed. However, most graphene flakes were disordered multilayers (see Figure S1 in supplementary information) [40]. Therefore, the estimation of the size distribution and number of layers in the flakes could not be conducted here. In Fig. 3(c), the diffraction image of the carbon onions looks like a ring pattern formed by many diffraction spots generated by different crystal orientations. In contrast, in Fig. 3(f), the diffraction pattern of a suspended graphene sheet shows distinct spots.

The EELS spectra of the carbon edge of the carbon onions and graphene flakes are correspondingly shown in Fig. 3(g) and (h). The excitation of the carbon K-shell electron (1s) to empty antibonding π^* and σ^* states is at ~285 eV and ~290 eV, respectively. In the case of the carbon onions the broad transition 1s-σ^* indicates a higher degree of disorder in this material than that of graphene flakes. The ratio between intensities of the absorption line 1s-π^* and 1s-σ^* (r) is related with the relative amount of sp^2 and sp^3 bonds in the material. [41] From EELS spectra, r ratio was found to be smaller in the case of the carbon onions than that of the graphene flakes, which indicates a higher disorder degree in carbon bonds.

Raman scattering, which is often used for monitoring the structural changes of carbon materials, provides additional information of the synthesized carbon in the SPP. Fig. 4(a), (b) and (c) show that both spherical carbon onions, graphene flakes and graphite electrode display three prominent peaks at ~1350 cm^{-1}, 1580 cm^{-1} and 2720 cm^{-1} known as D band, G band, and 2D band, respectively.[42,43] In Fig. 4(a), the D band of carbon onions is wider and much higher than that of graphene flakes, which

indicates that the carbon onions contain more disordered sp^2 carbon as well as defects.[43] The G band linewidth of the carbon onion is 58.6 cm^{-1}, which is wider than that of the graphene flakes where the value is 18.6 cm^{-1}. The spectrum of graphene flakes is similar to graphite electrode as presented in Fig. 4(c), which indicates that the graphene flakes were formed without destroying of carbon structure. The ratio between the intensities of D band (I_D) and G band (I_G) was additionally calculated. The I_D/I_G ratios in carbon onion and graphene flakes were 0.75 and 0.16, respectively. Due to the defects and disordered structure in carbon onion, the I_D/I_G ratio was higher. The distribution of the spectra collected within an area of about 1 mm^2 of graphene flakes is illustrated in Fig. 4(d)–(g). The analysis results showed that a precise control of the lateral sizes and the thickness of the graphene sheets cannot be obtained as was reported using a centrifugation procedure.[44,45]

3.2 *Plasma composition and parameters*

Optical emission spectra and images of plasma during the synthesis of carbon onion and graphene flakes are shown in the Fig. 5(a) and (b), respectively. The synthesis of the carbon onions resulted in burning-like white colored plasma, accompanied with a lot of bursting bubbles and radiant heat which were detected nearby the experimental beaker. In contrast, purple colored-plasma and small amount of tiny bubbles were observed during the synthesis of graphene flakes.

In Fig. 5(a), the optical emission spectrum resembles typical arc plasma spectrum from blackbody radiation punctuated by the emission of many excited carbon species such as C_2, C, CO and CH at high relative intensity. A large amount of carbon was generated from an erosion of electrodes before reacting with H and O atoms produced from the water dissociation, and generating CO and CH radicals. In the case of the graphene flakes production (Fig. 5 (b)), the peak at 247.8 nm corresponding to the excited C atom radical has a spectral intensity much lower than that of in the case of the carbon onions production. Other carbon radical peaks were not detected in the OES during the graphene flakes synthesis. The only observed radicals were H, O, and C atoms. The difference in the relative intensities indicated different contents of the gas bubbles surrounded by the solution and implied that gas bubbles formed during the synthesis of the carbon onions predominantly consist of carbon vapor, carbon monoxide, hydrogen and oxygen, whereas gas bubbles formed during the synthesis of the graphene flakes mainly consists of water vapor, small amount of hydrogen and oxygen gases, as well as carbon

monoxide. The electron excitation energy was estimated from the ratio of hydrogen emission intensities of Hα and Hγ, at wavelengths of 656.3 and 434.0 nm, respectively, and was found to be 0.6 and 1.4 eV in the case of plasma used for the graphene flakes and carbon onions synthesis, respectively (Table 1).

From the spectrum shown in the Fig. 5(a), the temperature, *T*, of the electrode tip was calculated by using Wien's law:

$$\lambda_{max} = \frac{2.898 \times 10^3}{T}$$

where λ_{max} is the wavelength corresponding to the maximum blackbody radiation distribution. In Fig. 5(a), λ_{max} is ~630 nm and *T* was calculated to be 4600 K, which is higher than the melting point (3825 K) and the boiling point (4489 K) of graphite.[46] The thermal energy of the gas in the vicinity of the electrode is 0.025 and 0.39 eV in plasma used for the graphene flakes and carbon onions synthesis, respectively. The surrounding water temperatures during the synthesis of carbon onions and graphene flakes were 373 K and 303 K, respectively (Table 1).

The input energy into plasma can be calculated using the current and voltage waveforms (see Figure S2 in the supplementary information) of the relation as shown below:

$$W = V \times I \times t$$

where *W, V, I* and *t* represents the energy, voltage, current and time, respectively. The calculated input energy per pulse in the case of the carbon onions formed at 60 kHz and 2 μs was 1.07×10^{-3} J and in the case of the graphene flakes produced at 20 kHz and 2 μs was 1.17×10^{-3} J. For a fixed frequency, the values of energies per second were 82.6 and 14.1 W for the formation of the carbon onions and graphene flakes, respectively. Although the energy per pulse was almost the same, the input power considerably differed for different carbon structures. The higher energy per second, which resulted in carbon onions synthesis, can explain the Joule effect which determines the heating of the graphite tip electrode and the blackbody radiation.

3.3 *Synthesis mechanism*

Based on these results and calculations, a synthesis mechanism of nanocarbon materials can be

developed. This is described in the following paragraphs and is summarized in Fig. 6.

3.3.1 *Plasma in water*

Mechanism of the bubbles formation is schematically represented in Fig. 6 (a). The initial input electrical energy is converted into thermal energy on the electrode surface, which heats water molecules and leads to vaporization. The gas bubbles nucleate at atmospheric pressure and plasma is generated inside the bubbles due to the high voltage applied between electrodes. Plasma is sustained and becomes stabilized under the bipolar pulsed voltage which generates a bipolar pulsed current. It is supposed that in the ionized gas a conduction channel is formed between electrodes by primary streamers.

In basic terms, the shape of plasma can be classified as corona discharge, glow discharge, spark discharge or arc discharge. In this experiment, spear-shaped electrodes were used, resulting in the plasma shape being very close to corona discharge with a high potential gradient. Nevertheless, the corona-shaped plasma was not dispersed and then streamers formed under atmospheric pressure due to high voltage and close inter-electrode gap in relatively high molecular density. Plasma can hardly progress to arc discharge using the bipolar power supply because of the short discharge time determined by the pulse width from 1 to 4 μs, which created non-equilibrium plasma (i.e. the temperature of the electrons is much higher than that of the ions). Thus, in this experiment plasma starts from corona discharge at the beginning and progresses to spark discharge with an energy accumulation at the side. The streamers formed inside the bubbles between the immersed electrodes in water generate ions and radicals from atoms and molecules, which accelerate the chemical reactions.

In this plasma, the ions were not strictly thermal (meaning the gas temperature) since the electric field during the plasma operation was about 20 kV cm^{-1}, due to a mean free path less than 1 μm at atmospheric pressure, which could result in average energies for ions of about 1 eV. The average electron energy corresponding to this electric field is about 2 eV.[47]

3.3.2 *Carbon onions synthesis*

In the case of the synthesis of the carbon onions (Fig. 6 (b)), the measured temperature of the electrode tip was 4600 K, which is higher than the melting and boiling points of graphite. Therefore, in zone O1, graphite was vaporized and carbon atoms expand from the center of the bubble to the outer regions due to the higher temperature. A small fraction of carbon atoms were sputtered from the graphite electrode by fast ions from plasma. Zone O2 was the region where the carbon vapor quenches because of the temperature gradient. The expanding carbon atoms gradually lost their energy and recombined with each other. At this point, the final shape of the carbon atoms combined into spherical onion because of the low surface energy. Zone O3 is the region where the remaining carbon atoms come in contact with water vapor forming H_2 and CO. In plasma phase the fast electrons were responsible for the C–C bond dissociation which required 6.5 eV energy, atomic, and molecular excitation and ionization processes. [48]

3.3.3 *Graphene flakes synthesis*

Based on the study carried out by Schabel and Martins, the exfoliation energy of graphite sheets was less than 1 eV.[49] The ion energy around 1 eV was enough to produce graphite exfoliation[47]. In Fig. 6 (c), the gas bubbles for the graphene flakes formation were smaller and have a lower temperature than that of the carbon onions formation due to lower input power. During the graphene flakes formation, the dissociation of the C–C bond occurred in zone G1 on the electrode surface because of the focused plasma energy despite the smaller amount of carbon vapor and the lower vapor pressure compared with the onion case. In zone G2, the graphene flakes were exfoliated due to the temperature gradient on the electrode surface, which implied that the energy in the zone was not sufficient to break the covalent C–C bonds but was sufficient to overcome the Van der Waals forces and separate the graphene layers. Zone G3 is the region where water vapor was transported from the bubble surface to the bubble center and where H and OH radicals were generated from the dissociation of water molecules in plasma. Dissociation, ionization, and excitation processes were produced by the fast electrons present in the plasma gas phase. The necessary energy to get excited carbon atoms from the electrode was about 12.5 eV because the exfoliation process needed 1 eV, the dissociation of the C–C bond needed 6.5 eV, and the excitation of carbon atom from ground state $^1P^0$ to excited state ^1S (See supplementary information Table S) required about 5 eV.[50] Although the photon energy in the SPP can

be about 5–6 eV, the photon flux was small and a photoexfoliation process of the graphite was negligible as compared with the exfoliation produced in plasma by ions and electrons.[51]

4. Conclusion

In summary, we have synthesized two different types of nanocarbon from graphite electrode: graphene flakes and carbon onions, by controlling the energy input from a bipolar pulsed power supply during solution plasma process in water. The energy per pulse delivered in plasma was similar for both carbon onions and graphene flakes synthesis. However, the power delivered in plasma was much higher in the case of carbon onion synthesis. The main process to produce the carbon onions is carbon vaporization due to Joule effect and carbon recombination assisted by plasma. In order to produce graphene flakes, the graphite electrode was exfoliated in plasma. The diameter of the carbon onions was ranged from 2 to 16 nm and the graphene flakes were hundreds of nanometers in size. Unfortunately a precise control of the lateral sizes and the thickness of the graphene flakes was not realized. The HRTEM, TEM, and EELS analysis confirmed the morphology and the structure of the graphene flakes and carbon onions. The Raman spectra of the graphene flakes indicated that it was disordered multilayers.

Acknowledgements

This work was supported in part by Core Research for Evolutional Science and Technology (CREST) of Japan Science and Technology (JST) Agency.

References

1 K. S. Novoselov, A. K. Geim, S. V. Morozov, D. Jiang, Y. Zhang, S. V. Dubonos, I. V. Grigorieva and A. A. Firsov, 2004, *Science*, 306, 666-9.

2 C. Lee, X. Wei, J. W. Kysar and J. Hone, 2008, *Science*, 321, 385-8.

3 M. D. Stoller, S. J. Park, Y. W. Zhu, J. H. An and R. S. Ruoff, 2008, *Nano Lett.*, 8, 3498-502.

4 R. R. Nair, P. Blake, A. N. Grigorenko, K. S. Novoselov, T. J. Booth, T. Stauber, N. M. R. Peres and A. K. Geim, 2008, *Science*, 320, 1308.

5 A. Reina, X. Jia, J. Ho, D. Nezich, H. Son, V. Bulovic, M. S. Dresselhaus and J. Kong, 2009, *Nano Lett.*, 9, 30-5.

6 A. A. Balandin, S. Ghosh, W. Bao, I. Calizo, D. Teweldebrhan, F. Miao and C. N. Lau, 2008, *Nano Lett.*, 8, 902-7.

7 R. van Noorden, 2011, *Nature*, 469, 14-16.

8 V. Chandra, J. Park, Y. Chun, J. W. Lee, I. C. Hwang and K. S. Kim, 2010, *ACS Nano*, 4, 3979-86.

9 W. H. Lee, J. Park, Y. Kim, K. S. Kim, B. H. Hong and K. Cho, 2011, *Adv. Mater.*, 23, 3460-4.

10 K. S. Kim, Y. Zhao, H. Jang, S. Y. Lee, J. M. Kim, K. S. Kim, J. H. Ahn, P. Kim, J. Y. Choi and B. H. Hong, 2009, *Nature*, 457, 706-10.

11 X. Li, W. Cai, J. An, S. Kim, J. Nah, D. Yang, R. Piner, A. Velamakanni, I. Jung, E. Tutuc, S. K. Banerjee, L. Colombo and R. S. Ruoff, 2009, *Science*, 324,1312-4.

12 Z. Sun, Z. Yan, J. Yao, E. Beitler, Y. Zhu and J. M. Tour, 2010, *Nature*, 468, 549-52.

13 P. W. Sutter, J. I. Flege and E.A. Sutter, 2008, *Nat. Mater.*, 7, 406-11.

14 Y. Y. Shao, J. Wang, M. Engelhard, C. M. Wang and Y. H. J. Lin, 2010, *Mater. Chem.*, 20, 743-8.

15 Y. W. Zhu, M. D. Stoller, W. W. Cai, A. Velamakanni, R. D. Piner, D. Chen and R. S. Ruoff, 2010, *ACS Nano*, 4, 1227-33.

16 G. Williams, B. Seger and P. V. Kamat, 2008, *ACS Nano*, 2, 1487-91.

17 L. Grande, V. T. Chundi, Di Wei, C. Bower, P. Andrew and T. Ryhanen, 2012, *Particuology*, 10, 1-8.

18 C. Karuwan, C. Sriprachuabwong, A. Wisitsoraat, D. Phokharatkul, P. Sritongkham and A. Tuantranont, 2012, *Sensors and Actuators B: Chem.*, 161, 549-555.

19 M. Cheng, R. Yang, L. Zhang, Z. Shi, W. Yang, D. Wang, G. Xie, D. Shi and G. Zang, 2012,

Carbon, 50, 2581-7.

20 G. Nandamuri, S. Roumimov and R. Solanki, 2010, *Appl. Phys. Lett.*, 96, 154101.

21 K. Ostrikov, E. C. Neyts and M. Meyyappan, 2013, *Advances in Physics*, 62, 113.

22 O. Volotskova, I. Levchenko, A. Shashurin, Y. Raitses, K. Ostrikovand and M. Keidar, 2010, *Nanoscale*, 2, 2281.

23 N. Sano, H. Wang, I. Alexandrou, M. Chhowalla, K. B. K. Teo and G. A. J. Amaratunga, 2002, *App. Phys.*, 92, 2783-8.

24 N. Sano, 2005, *Carbon*, 43, 450-3.

25 M. V. Antisari, R. Marazzi and R. Krsmanovic, 2003, *Carbon*, 41, 2393-401.

26 N. Sano, J. Nakano and T. Kanki, 2004, *Carbon*, 42, 686-8.

27 G. Xing, S. Jia and Z. Shi, 2007, *Carbon*, 45, 2584-8.

28 C. Poonjarernsilp, N. Sano, T. Charinpanitkul, H. Mori, T. Kikuchi and H. Tamon, 2011, *Carbon*, 49, 4920-7.

29 H. Lange, M. Sioda, A. Huczko, Y. Q. Zhu, H. W. Kroto and D. R. M. Walton, 2003, *Carbon*, 41, 1617-23.

30 J. Hieda, N. Saito and O. Takai, 2008, *J. Vac. Sci. Technol. A*, 26, 854-6.

31 O. L. Li, J. Kang, K. Urashima and N. Saito, 2013, *J. Inst. Electrostat. Jpn.*, 37, 22-27.

32 A. Watanaphanit and N. Saito, 2013, *Polym. Degrad. Stabil.*, 98, 1072-80.

33 P. Pootawang, N. Saito, O. Takai and S. Y. Lee, 2012, *Nanotech.*, 23, 395602.

34 S. P. Cho, M. A. Bratescu, N. Saito and O. Takai, 2011, *Nanotech.*, 22, 455701.

35 M. A. Bratescu, S. P. Cho, O. Takai and N. Saito, 2011, *J. Phys. Chem. C*, 115, 24569.

36 J. Kang, O. L. Li and N. Saito, 2013, *Nanoscale*, 60, 292-8.

37 C. Miron, M. A. Bratescu, N. Saito and O. Takai, 2010, *Plasma Chem. Plasma Process.*, 30, 619-631.

38 F. Torrisi, T, Hasan, W. Wu, Z. Sun, A. Lombardo, T. S. Kulmala, G. W. Hsieh, S. Jung, F. Bonaccorso, P. J. Paul, D. Chu, A. C. Ferrari, 2012, *ACS Nano*, 6, 2992-3006.

39 O. M. Marago, F. Bonaccorso, R. Saija, G. Privitera, P. G. Gucciardi, M. A. Lati, G. Calogero, P. H. Jones, F. Borghese, P. Denti, 2010, *ACS Nano*, 4, 7515-23.

40 M. Lotya, Y. Hernandez, P. J. King, R. J. Smith, V. Nicolosi, L. S. Karlsson, F. M. Blighe, S. De, Z. M. Wang, I. T. McGovern, G. S. Duesberg and J. N. Coleman, 2009, *J. Am. Chem. Soc.*, 131, 3611-20.

41 J. Bruley, D. B. Williams, J. J. Cuomo, D. P. Papas J., 1995, *Microscopy,* 180, 22

42 A. K. Gupta, T. J. Russin, H. R. Gutierrez and P. C. Eklud, 2009, *ACS Nano*, 3, 45-52.

43 A.C. Ferrari, F. C. Meyer, V. Scardaci, C. Casiraghi, M. Lazzeri, F. Mauri, S. Piscanec, D. Jiang, D. S. Novoselov, S. Roth and A. K. Geim, 2006, *Phys. Rev. Lett.*, 97, 187401, 1-4.

44 A. A. Green, M. C. Hersam, 2009, *Nano Lett.*, 9, 4031-6.

45 F. Bonaccorso, A. Lombardo, T. Hasan, Z. Sun, L. Colombo, A. C. Ferrari, 2012, *Materials Today*, 15, 564-89.

46 D. R. Lide. CRC handbook of chemistry and physics 90th edn. CD-ROM version; 2010.

47 N. Y. Babaeva and M. J. Kushner, 2011, *Plasma Sources Sci. Technol.*, 20, 035017.

48 Darwent B deB, 1970, *Bond Dissociation Energies in Simple Molecules*, NSRDS-NBS 31

49 M. C. Schabel, J. L. Martins, 1992, *Phys. Rev. B*, 46, 7185.

50 http://physics.nist.gov/PhysRefData/ASD/lines_form.html Accessed 4 March 2014

51 S. Dhar, A. R. Barman, G. X. Ni, X. Wang, X.F. Xu, Y. Zheng, S. Tripathy, Ariando, A. Rusydi, K. P. Loh, M. Rubhausen, A. H. C. Neto, B. Zyilmaz, T. Venkatesan, 2011, *AIP Adv.*, 1, 022109.

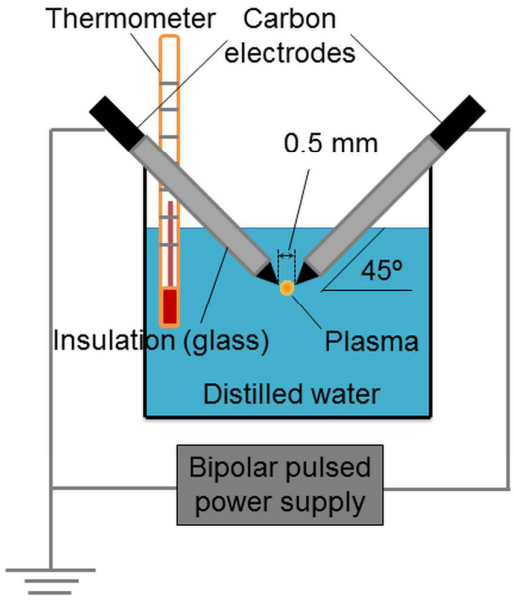

Fig. 1. Experimental setup for the solution plasma processing.

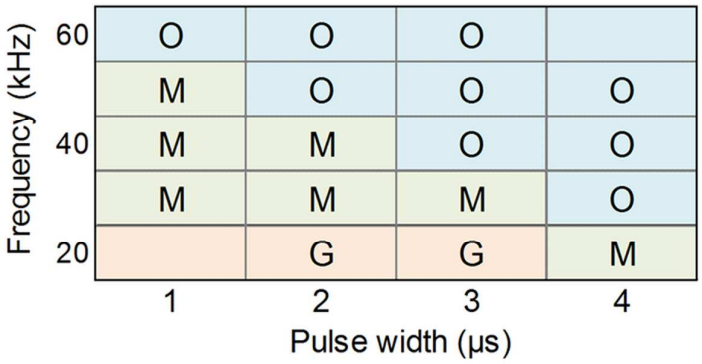

Fig. 2. Nanocarbon structural changes versus the experimental conditions measured from the waveforms of the bipolar pulsed power supply. The symbols are as follows: G: graphene flakes; O: onion structure; M: mixture of the carbon in both forms.

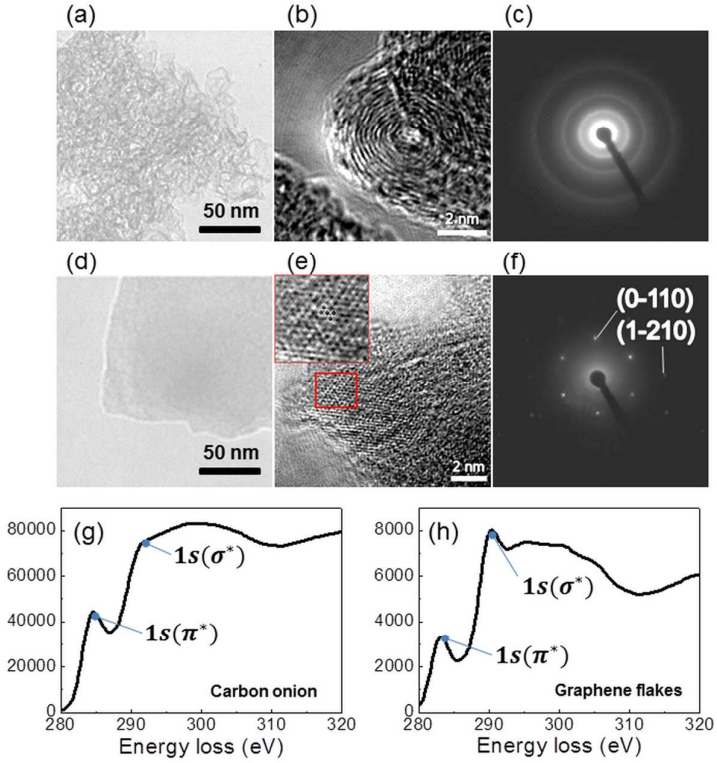

Fig. 3. Morphology images and diffraction patterns observed by TEM, HRTEM and SAED. (a) TEM image, (b) HRTEM image, and (c) SAED pattern of carbon onions synthesized at 60 kHz frequency and 2 μs pulse width and (d) TEM image, (e) HRTEM image, and (f) SAED pattern of graphene flakes obtained at 20 kHz frequency and 2 μs pulse width. Carbon edge of the EELS spectra corresponding to (g) carbon onions and (h) graphene flakes. The excitation of the carbon K-shell electron to empty antibonding π* and σ* states is at ~285 eV and ~290 eV, respectively. The carbon edge is at 284 eV.

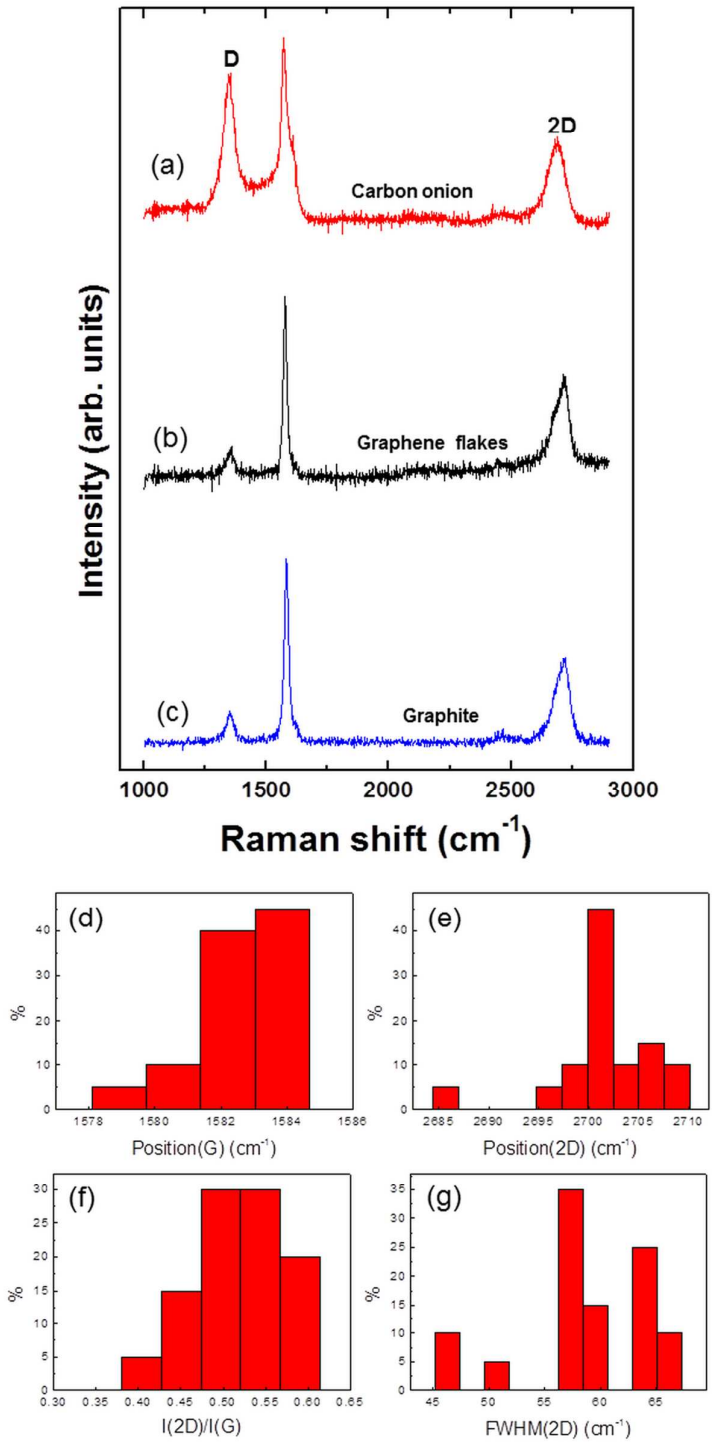

Fig. 4. Raman spectra of (a) carbon onion, (b) graphene flakes, and (c) graphite electrode on SiO_2/Si substrate measured a laser excitation wavelength at 532 nm. Statistical analysis of the Raman spectra of the graphene flakes within an area of about 1 mm^2 of (d) G band, (e) 2D band position, (f) ratio I_{2D}/I_G, and (g) FWHM of the 2D band. The *y*-axis in the plots (d)-(g) represents the percentage of the total number of measured spectra.

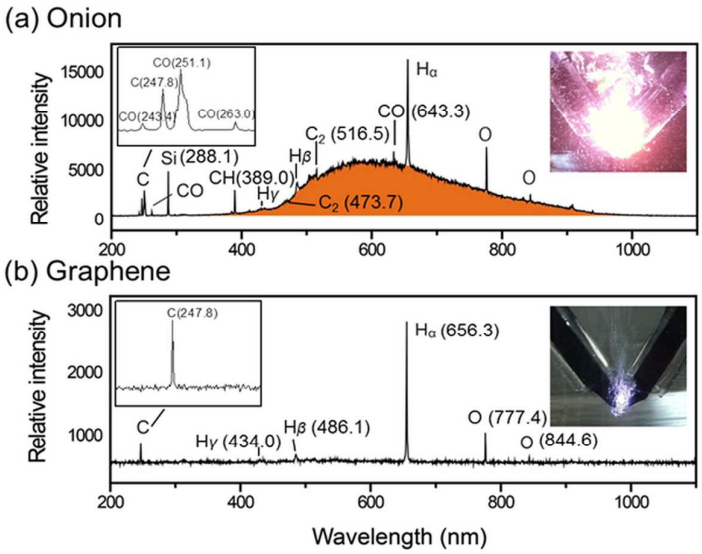

Fig. 5. Optical emission spectra and images of plasma generated during the synthesis of (a) carbon onion and (b) graphene flakes (Spectra identification is given in the Table S in the Supporting Information). On the right upper corners, images of plasma are inserted.

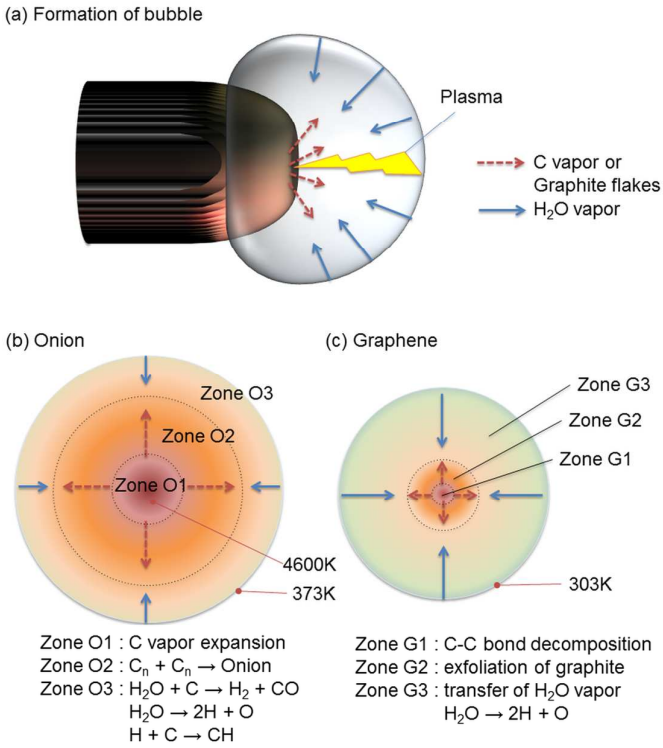

Fig. 6. (a) Proposed mechanisms for the bubble formation on the graphite electrodes discharged in distilled water. Reaction zones according to temperature distributions during the synthesis of (b) carbon onions and (c) graphene flakes.

Table 1. Parameters of plasma derived from the experimental data.

Parameter	Graphene flakes	Carbon onions
Electrode temperature *T*	300 K 0.025 eV	4600 K 0.39 eV
Electron excitation energy	6932 K 0.6 eV	16306 K 1.4 eV
Input energy in plasma	At 20 kHz and 2 μs 1.17×10^{-3} J	At 60 kHz and 2 μs 1.07×10^{-3} J
Power	14.1 W	82.6 W